Fano resonances in chalcogen-doped silicon

E. Janzén,* G. Grossmann, R. Stedman, and H. G. Grimmeiss
Department of Solid State Physics, University of Lund, P.O. Box 118, S-221 00 Lund, Sweden
(Received 17 December 1984)

Photoexcitation spectra showing structure in the continuum part due to resonant electron-phonon interaction are presented for various centers related to S, Se, and Te in silicon. Theoretical aspects of these Fano resonances are discussed to provide a basis for the interpretation and analysis of results. The analysis allows binding energies to be assigned to several bound states not observable by direct optical excitation. A theoretical model is presented which offers an explanation for the differences between Fano resonances in absorption and photoconductivity spectra. A clear case of oscillating photoconductivity in Si:Te is also presented and interpreted in terms of cascade decay involving optical phonons together with enhanced capture of the slowest conduction electrons at low temperature.

I. INTRODUCTION

In a previous paper[1] optical spectra of several donors related to sulfur and selenium in silicon were presented and analyzed. We refer to that paper for details of spectra, classification of lines, labeling of centers, and experimental procedures. Only direct transitions to bound excited states were considered there. Here we turn to spectral structure above the ionization limit to examine the information such structure contains. In particular, the binding energies of bound electronic states to which direct optical transitions are forbidden can be derived from resonances in the continuum region.

A typical line spectrum and accompanying continuum are shown in Fig. 1(a), which is for the photoresponse of the center S^0. Between 330 and 380 meV there is distinct structure due to Fano resonances dealt with here. These resonances are named after Fano, who first gave a full theoretical account of similar resonances in atomic spectra.[2] Such resonances can occur whenever the zeroth-order description of a system includes a discrete state degenerate with a continuum [Fig. 2(a)]. Any small interaction between the discrete state and the continuum will then mix them strongly in the neighborhood of the degeneracy, and thereby give rise to interference effects in spectra. In our case the continuum comprises electronic states above the conduction-band minimum, and the discrete state describes an electron in a bound excited state of the donor together with a phonon [Fig. 2(b)]. We may regard the interaction as inelastic scattering of electrons between continuum states and a bound state via particular phonons. While the phonon state is actually not discrete, rather stringent selection rules restrict the phonons involved to a very narrow energy range. A typical Fano resonance in the continuum spectrum of a donor is illustrated in Fig. 2(c).

Selection rules for phonons are discussed in Sec. II, together with some other theoretical aspects. Further, a theoretical model explains the differences between the line shapes of Fano resonances in absorption spectra and photoconductivity spectra.

Fano resonances have previously been observed in silicon for shallow substitutional centers—P, As, Sb (though the original interpretation was different) (Ref. 3), B, Al, Ga (Refs. 4 and 5), and In (Ref. 5)—and for the centers here referred to as S^0 and S_2^0.[6] We have observed them for chalcogen donors of varying ground-state depths and different symmetries: S^0, Se^0, Te^0, S_2^0, Se_2^0, and Te^+. Our experimental results are presented and commented on in Secs. III and IV. A brief account of our earlier results was given in Ref. 7.

Another phenomenon associated with the electron-phonon interaction appeared in our photoconductivity and Fourier photoadmittance spectroscopy[8] (FPAS) spectra for Te^0. This is oscillating photoconductivity, discussed in Sec. V. An important feature of the explanation discussed there is the large cross section of donors at low temperatures for capture of conduction electrons close to the band minimum via the upper excited states of these centers.

II. SOME THEORETICAL ASPECTS OF THE PRESENT FANO RESONANCES

A. Selection rules and general considerations

The bound electronic states involved in Fano resonances are sufficiently shallow that they may be regarded as built up of Bloch states from a fairly narrow region around each band minimum, and the same applies to the continuum states to which they couple. So the matrix element for interaction between states via a phonon may be expanded in terms of matrix elements for electron-phonon interactions between Bloch states from the "valleys" around the six equivalent band minima.

The first selection rule corresponds to momentum conservation. It requires a phonon wave vector to be approximately equal to a vector joining different minima. These intervalley phonons are denoted by the vectors f and g [Figs. 2(d) and 3]. Wave vectors close to zero are also permitted by this rule, but are excluded on other grounds (see

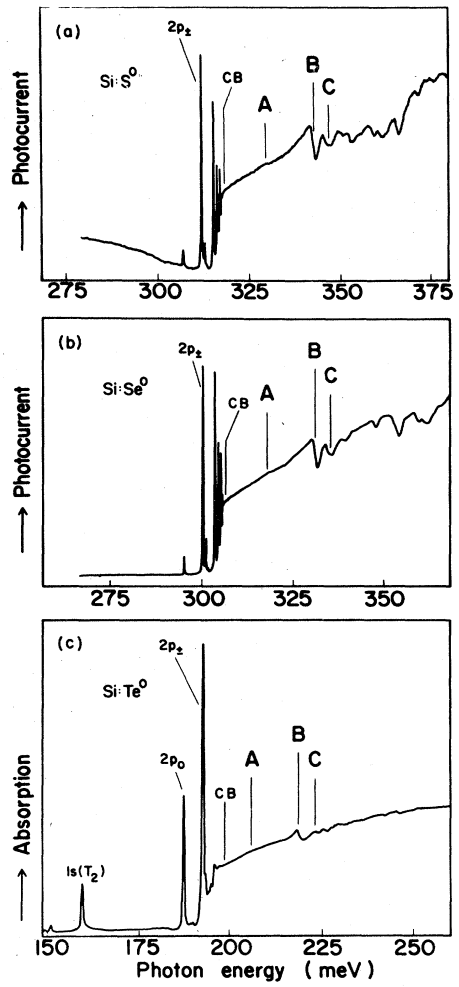

FIG. 1. Photoexcitation spectra of S^0, Se^0, Te^0 centers in silicon. *A*, *B*, and *C* mark the excitation energy of the $1s(T_2)$ state plus the energies of three different intervalley phonons, see Fig. 2(d). (a) Photoconductivity spectrum of S^0. The resolution is 0.06 meV and the temperature 20 K. (b) Photoconductivity spectrum of Se^0. The resolution is 0.03 meV and the temperature 6 K. (c) Absorption spectrum of Te^0. The resolution is 0.25 meV and the temperature 10 K.

below). This selection rule is experimentally confirmed by the anomalous broadening of the $2p_0$ state of Bi in silicon and by the marked stress-induced energy dependence of this broadening.[9] From observations on the bound states[1] of the centers we are considering, we also conclude that decay via intervalley phonons to a lower excited bound state is a strong process with a pronounced effect on lifetimes of states.

The allowed phonon wave vectors will actually be distributed around the nominal *f* and *g* values in accordance with the spread in **k** space of the electronic single-valley wave functions these phonons link. The width of this distribution can be estimated using the effective-mass wave functions of the bound states—transformed to **k** space—and the effective masses of the conduction band. It turns out that for bound states and continuum states separated

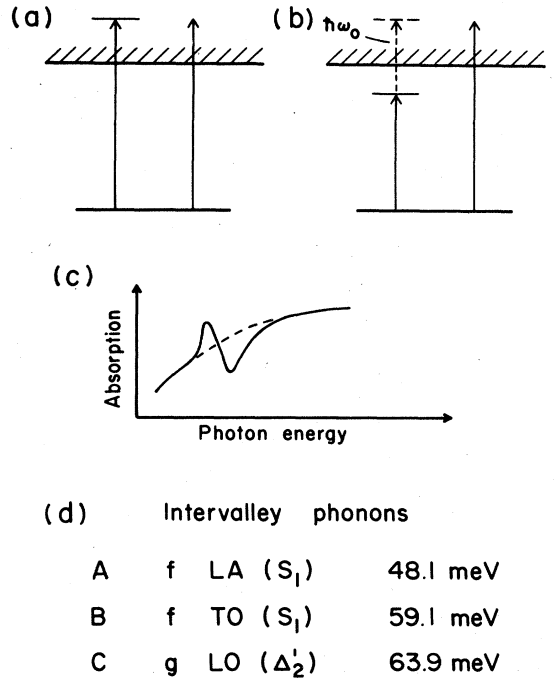

FIG. 2. Schematic view of Fano resonances. For details, see text.

by about 60 meV—the energy of the dominant intervalley phonons, see Fig. 2(d) and below—the width of the phonon distribution is about 0.15 reciprocal-lattice units ($2\pi/a$), irrespective of which states are involved. The broadening of a deeper excited bound state is counteracted by the narrowing of the corresponding continuum state. Once the appropriate phonon branches have been found, we can establish corresponding approximate energy widths for the phonon distributions, and show how these energy widths affect observed Fano resonances.

The second selection rule concerns phonon symmetry and its relation to the electron momentum transfer. The

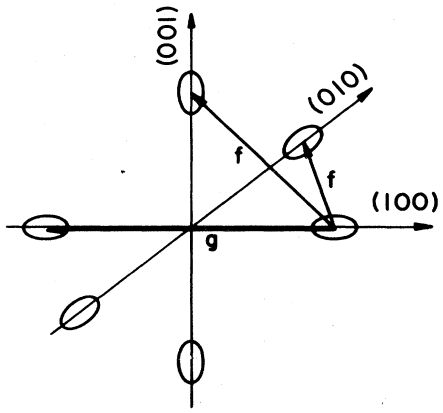

FIG. 3. Schematic view of the constant energy surfaces of the six conduction minima in silicon showing the two possible types of intervalley scattering.

latter may be taken for Bloch waves at the minima, with the phonon wave vectors exactly 0, f, or g. That is, it is assumed that variation of electron-phonon matrix elements in the wave-vector regions under consideration can be disregarded. Results may be taken from group-theoretical treatments of the related problem which concerns scattering of conduction electrons by phonons in silicon.[10,11] The only allowed branches for f phonons are TO(S_1) and LA(S_1) and for g phonons LO(Δ_2'). According to Asche and Sarbei,[12] the f TO and g LO phonons couple with comparable strength to electrons, while the f LA interaction is weaker. The energies of these three intervalley phonons are given in Fig. 2(d), and derived in Appendix A. Harrison[13] found that optical phonons of wave vector close to zero may be disregarded.

Having identified the relevant phonon dispersion branches, the estimates previously given of typical wave-vector uncertainties can now be converted to energy widths. For the g LO phonon the width is about 1.5 meV and for the f TO phonon about 1 meV—and it is emphasized once again that these estimates are very rough. For f LA phonons the dispersion and the dynamic structure factor for electron scattering are both complicated by the circumstance that the branch in question has a crossover singularity nearby, along XW (cf. Table I in Ref. 14). In such a neighborhood, both the phonon energy and polarization vary quite rapidly, and the corresponding phonon energy width may be expected to be rather larger than for the f TO and g LO phonons.

The strength of the coupling of the continuum states to the bound states via the electron-phonon interaction is affected by multiplicity factors, both as regards phonons and as regards the degeneracy of electron states. f coupling contains a factor 4 where g coupling contains a factor 1, corresponding to the fact that any valley can couple to four others by f processes, but to only one other by a g process. If the f TO and g LO phonons interact equally strongly with electrons in intervalley scattering,[12] this indicates that the total f interaction between multivalley states is several times as strong as the total g interaction. A further strength factor, which occurs in coupling to components of (ns) states split by valley-orbit interaction, is the multiplicity of the component: 1 for A, 2 for E, and 3 for T. Here we assume the split states simply to be different linear combinations of the same single-valley components.

A further important aspect to be considered here concerns optical excitation of phonon replicas of bound states. We believe that the transition probability for such excitation—a second-order process—is small for chalcogen centers in silicon, relative to probabilities for direct transitions to electronic bound or continuum states. The interaction of electrons with phonons in a homopolar crystal such as silicon is probably weak, and furthermore, there is no direct evidence of phonon replicas in optical spectra for chalcogen centers in silicon. The lowest excited states of singly ionized chalcogen centers are sufficiently deep that their phonon replicas should occur well below the continuum boundary—and actually, it turns out, in spectrally empty regions—but we have found no trace of excitation to such states.

Finally, it should be noted that we found the resonance line shapes in photoconductivity to be quite independent of impurity concentration. This indicates that the resonances are indeed related to the excitation process at a single impurity and not to the subsequent carrier transport through the crystal, a conclusion already stated by Humphreys *et al.*[6]

B. Resonance shapes

Our model for the line shape of a single Fano resonance is based on the assumption that we may disregard the interaction with all phonons that do not satisfy the resonance conditions. This seems justified as we do not expect nonresonant phonons to contribute to the sharper features of the Fano resonances. We are thus faced with the problem of two interacting continua; one is the electron conduction band (CB) and the other the narrow band of states describing a bound electron and an intervalley phonon of appropriate symmetry (BE-P). The continua are coupled by the electron-phonon interaction, $V_{e\text{-ph}}$, which describes the scattering of electrons between the conduction band and the bound electronic state via phonon emission or absorption.

In order to solve this problem we consider a further simplification. We model the narrow BE-P continuum by a discrete BE-P state (ϕ_0) with energy ϵ_0 broadened by a coupling U to a background BE-P continuum. Allowing the electron-phonon interaction $V_{e\text{-ph}}$ to couple electrons to phonons only via this discrete state, we simulate the interaction with a narrow BE-P band. One may interpret this technical procedure in more physical terms and consider the scattering to be due to some local discrete phonon mode, which is broadened by interaction with a thermal background into which it may decay. Due to the interactions U and $V_{e\text{-ph}}$, the true eigenstates of the system will be appropriate linear combinations of the discrete state and the continua. In zeroth order we have optical transitions from the initial state $|i\rangle$—the ground state of

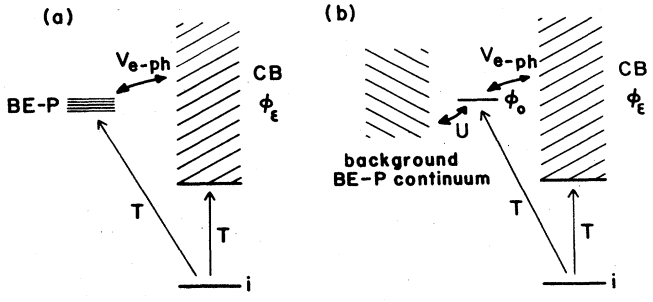

FIG. 4. Schematic view of present model. (a) The electronic CB continuum couples to the narrow BE-P continuum via the electron-phonon interaction $V_{e\text{-ph}}$. (b) Simplified model where the narrow BE-P continuum is simulated by a discrete state $|\phi_0\rangle$ broadened by a coupling U to a background BE-P continuum.

the donor with energy E_i—to the CB and to the discrete Be-P state, the probability for the latter most likely rather small (cf. preceding section). The coupling ($V_{e\text{-ph}}$ and U) of these zeroth-order states then leads to the interference effects which are observed as resonances. A schematic view of our model is shown in Fig. 4, where the CB states, as discussed below, are denoted by $|\phi_\epsilon\rangle$ and T is the dipole transition operator.

In this model we have obtained an easily solvable problem, where the true continuum character of the phonons is retained, albeit at the price of approximating $V_{e\text{-ph}}$ by an effective interaction, i.e., we now ignore the detailed $\mathbf{k}$ dependence of the scattering matrix elements which, however, was taken into account when selecting the phonons fulfilling the resonance conditions. Whereas all transitions contribute to the absorption spectrum, we will calculate the photoconductivity spectrum taking only those transitions into account that actually leave an electron in the conduction band. We also assume that all electrons, once excited to the conduction band, contribute to photoconductivity and disregard all problems associated with carrier transport.

In the limit that the narrow BE-P continuum is replaced by a truly discrete state, $U=0$, absorption and photoconductivity yield the same spectrum as shown below, i.e., every photon absorbed yields an electron in the conduction band. A truly discrete state would describe a bound electron together with a discrete, local phonon, and this state has no other choice than to decay into the CB continuum; the local phonon cannot move away and leave a bound electron at the impurity site. (In a recent paper Jauho and Minnhagen[15] explore this interaction with a discrete phonon focusing their model study, however, on the resulting multiphonon structure rather than on the detailed line shape of the observed one-phonon resonances.) An immediate consequence of a true BE-P continuum is that the excitation may decay into the bound-electron-phonon channel. Absorption and photoconductivity spectra will then differ, reflecting the fact that there are different final-state channels for the initial excitation process, resulting in either a CB electron or a bound electron together with a phonon that has left the center.

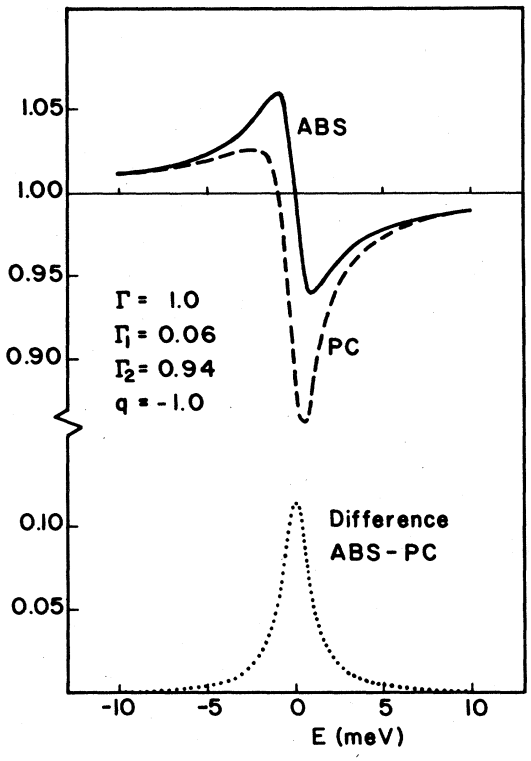

FIG. 5. Line shapes of Fano resonances in absorption (solid line) and photoconductivity (dashed) as obtained within the simplified model are shown together with their Lorentzian difference (dotted). The spectra are normalized to the background spectrum $|T_\omega|^2$.

The problem of a discrete state interacting with two continua was already considered by Fano[2] for the case of absorption. The calculation of the photoconductivity spectrum, however, is rendered much easier if we solve our model problem within scattering theory. This elegant approach, treating very similar problems, is discussed at length by Almbladh and Hedin in a recent review article.[16] The absorption spectrum is given by the golden-rule expression ($\hbar=1$)

$$I_a(\omega)=2\pi\sum_f |\langle f|T|i\rangle|^2\delta(E_i+\omega-E_f) \tag{1}$$

with the optical dipole-transition operator T and where we sum over all final states $|f\rangle$ with energy E_f. The photoconductivity spectrum, on the other hand, is given by

$$I_{\rm pc}(\omega)=2\pi\sum_{\mathbf{k}} |\langle \epsilon_{\mathbf{k}}|T^+|i\rangle|^2\delta(E_i+\omega-\epsilon_{\mathbf{k}}) \tag{2}$$

in terms of the scattering amplitudes, i.e., the matrix elements of the T^+ operator. The T^+ operator [cf. Eq. (A9)] includes the initial optical excitation and the subsequent multiple scattering between the zeroth-order states coupled by the interactions. Taking the matrix elements with the states $|\epsilon_{\mathbf{k}}\rangle$, we then select only those processes that actually leave an electron in the CB. In general, the CB states are labeled by $\mathbf{k}$; in the following, however, we will only consider the dominant symmetry channel, i.e., we assume the states of the CB continuum to be functions of energy only, we denote then $|\phi_\epsilon\rangle$ and take them to be δ-function normalized in the energy variable. In this way we simplify the evaluation but only disregard an additional slowly-varying contribution to the spectra. Thus, the photoconductivity spectrum is given by

$$I_{\rm pc}(\omega)=2\pi\int d\epsilon\,|\langle\phi_\epsilon|T^+|i\rangle|^2\delta(E_i+\omega-\epsilon)\,. \tag{3}$$

As the solution of this model problem *per se* is rather straightforward,[16] we give the details of the somewhat lengthy evaluation of the above expressions in Appendix B, where we find the following results for absorption:

$$I_a(\omega)=|T_\omega|^2\left[\frac{\Gamma_2}{\Gamma}+\frac{\Gamma_1}{\Gamma}\frac{(E+\Gamma q)^2}{E^2+\Gamma^2}\right] \tag{4}$$

and for photoconductivity:

$$I_{\rm pc}(\omega)=|T_\omega|^2\left[\frac{\Gamma_2^2+(E+\Gamma_1 q)^2}{E^2+\Gamma^2}\right], \tag{5}$$

where

$$T_\omega=\langle i|T|\phi_\epsilon\rangle|_{\epsilon=\omega} \tag{6}$$

is the optical transition matrix element between the ground state and the zeroth-order CB and where the zero of energy has been taken at the energy of the donor ground state. The total "width" Γ is the sum of the partial widths $\Gamma_1(\omega)=\pi|V_{e\text{-ph}}(\omega)|^2$ and $\Gamma_2(\omega)=\pi|U(\omega)|^2$ which the discrete level acquires due to the couplings $V_{e\text{-ph}}$ and U, respectively. $E=\omega-\epsilon_0-\Delta$ measures the energy relative to the center of the resonance defined by $\epsilon_0-\Delta$ and the Fano parameter q, finally, is defined by Eq. (A8). If the interaction matrix elements only vary slowly on the scale of the resonance width, we may consider q and the widths Γ_i to be approximately constant.

The absorption spectrum is seen to consist of a smooth background onto which a Fano line shape is superimposed. The results for absorption and photoconductivity are related by

$$I_{\rm pc}(\omega)=I_a(\omega)-|T_\omega|^2\pi\frac{\Gamma_1\Gamma_2}{\Gamma}(1+q^2)\left[\frac{1}{\pi}\frac{\Gamma}{E^2+\Gamma^2}\right], \tag{7}$$

where the energy-dependent expression in large parentheses is a Lorentzian line shape. We will here take q as a fitting parameter since the present model does not allow a more detailed evaluation. Whatever its value, however, we see from Eq. (7) that $I_{\rm pc}$ is obtained from I_a by subtraction of a—in our model Lorentzian—term whose amplitude is proportional to the product of the probability of an electron being scattered into a bound state by phonon emission (Γ_1) and of the probability for the (discrete) phonon to decay into the background continuum (Γ_2).

Consider the limiting case of $U=0$, i.e., a truly discrete BE-P state. The total width Γ now equals Γ_1 ($\Gamma_2=0$), i.e., it is only due to the coupling of the discrete state to the CB continuum, and we find $I_a=I_{\rm pc}$, as discussed above. The discrete BE-P must eventually decay into the CB continuum, a local phonon cannot leave the center. In the other limit, $V_{e\text{-ph}}=0$, we have $\Gamma=\Gamma_2$ and

$$I_a(\omega)=|T_\omega|^2+|T_0|^2\frac{1}{\pi}\frac{\Gamma}{E^2+\Gamma^2} \tag{8}$$

with $T_0=\langle\phi_0|T|i\rangle$ and for photoconductivity

$$I_{\rm pc}(\omega)=|T_\omega|^2. \tag{9}$$

Absorption is determined by mutually independent transitions to the electronic continuum and to the discrete BE-P state whose Lorentzian broadening with width Γ_2 models the narrow BE-P continuum. Photoconductivity, on the other hand, depends on transitions to the electronic continuum alone.

The Fano line shape of the absorption spectrum—the second term in Eq. (4)—has its maximum and minimum at $E=\Gamma/q$ and $E=-\Gamma q$, respectively. Taking the leftmost pronounced resonance of Fig. 7 as an example (Te^0, $1s(T_2)+f$ TO phonon), we see that q must be negative and as an estimate we take $q\simeq-1$. Here we have compared the line shape with the line shapes given in Fano's paper,[2] and this value also agrees with our expectation that the phonon replica will not contribute any noticeable excess transition probability to the absorption spectrum (cf. Ref. 2). The extrema are about 2 meV apart, thus (for $q\simeq-1$) $\Gamma\simeq1$ meV. From the ratio of the maximum and minimum values of the full spectrum shown in Fig. 1(c) and with the proviso that the slowly-varying contribution which was disregarded above is small, we further estimate $\Gamma_1\simeq0.06$ meV and $\Gamma_2\simeq0.94$ meV—this latter estimate agrees well with the estimate of Sec. II A. Taking the transition probability to the continuum as constant, we obtain for this set of parameters the line shapes shown in

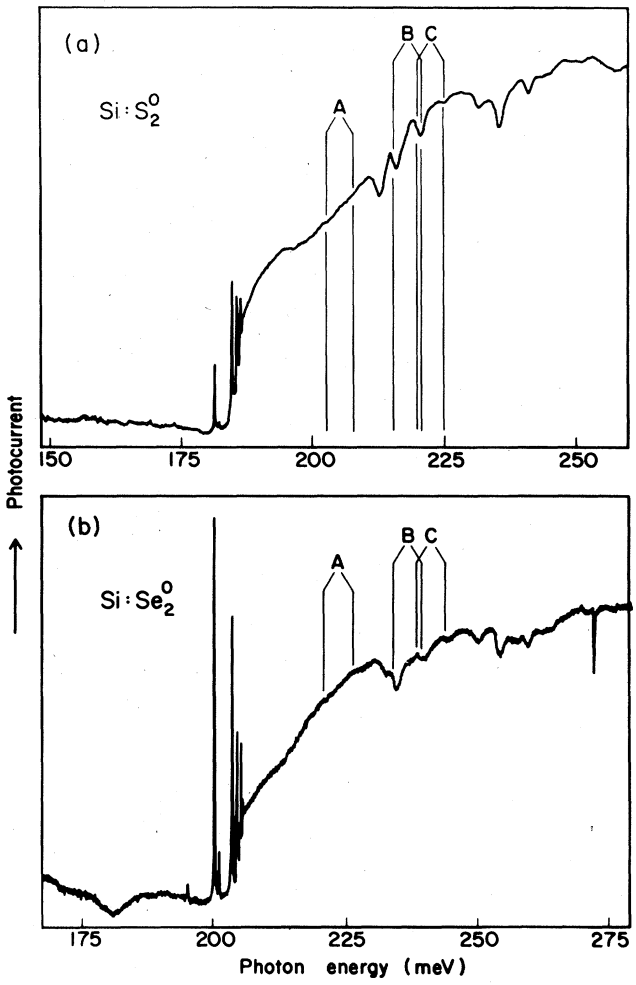

FIG. 6. Photoconductivity spectra of (a) S_2^0 and (b) Se_2^0. *A*, *B*, and *C* mark the excitation energy to the lowest excited states observable in no-phonon absorption [$1s(E^-)$ and $1s(A_1^-)$] plus the energy of the three different intervalley phonons, see Fig. 2(d). In (a) the resolution is 0.03 meV and the temperature 6 K. In (b) the resolution is 0.12 meV and the temperature 8 K. The dip at 272 meV in (b) is due to loss of photons when electrons are excited to the $1s(T_2)$ state of Se^0.

Fig. 5. Due to the crudeness of our model, we have not attempted any more detailed fit to experiment, but are satisfied that the essential features are given qualitatively correctly. The result indicates that the resonance width is essentially determined by the width of the narrow phonon band, while the coupling to the electronic CB contributes to the width only to a lesser degree.

For negative q the antiresonance of absorption lies at higher energy than the center of the resonance at $E=0$; in photoconductivity the antiresonance is shifted closer to $E=0$. The positive feature of the resonance is suppressed in photoconductivity while the dip is more pronounced, in agreement with the experimental data.

Recently an explanation for the difference in shape between the absorption and photoconductivity spectra was given by Chang and McGill,[17] which attributed this difference to transitions to a band of phonon replicas with a width similar to that of the resonances. These replicas were not coupled to the electronic CB and would consequently only contribute to absorption. The fact that phonon replicas, as mentioned above, have not been observed for these systems indicates, however, that they are either too weak or too broad to be detected. For these rather deep impurities with a correspondingly greater spread of their ground state in **k** space, selection rules would in fact not restrict possible phonon replicas to be as narrow as the resonance widths. But this they would have to be if they were to account for the difference in shape between absorption and photoconductivity. Including the decay mechanism discussed above, however, there is no need to assume substantial transition probabilities to narrow phonon replicas.

The most prominent features of our resonances—the minima—were used to derive approximate values for the energies of associated bound states which are not seen in line spectra below the continuum limit. The method we employ assumes that factors which tend to shift an observed minimum with respect to $(E_b+E_{\rm ph})$—where E_b and $E_{\rm ph}$ refer to the bound state and mean phonon concerned—do not vary sharply between neighboring resonances. Then, by comparing the minimum of a resonance that corresponds to an unobserved bound electronic level with a neighboring minimum of a resonance that corresponds to an observed line, the energy difference of the respective bound electronic states can be derived. It may be noted that the phonon energy does not need to be known exactly in this procedure, and furthermore, that the procedure can be tested on many pairs of resonances for which the corresponding line energies are both known.

C. Oscillating photoconductivity

There is another way in which interaction of electrons and optical phonons can lead to structure in spectral continua, besides the Fano resonances considered hitherto. This is the phenomenon of oscillating photoconductivity (see Marfaing[18] and references therein), which depends in the first place on the predominance of a relatively narrow band of optical phonons in the process by which electrons photoexcited well up in the conduction band lose energy. If the mean energy of the optical phonons which interact most strongly with conduction electrons is $\hbar\omega$, electrons initially at energy E_p above the conduction-band minimum may be quickly slowed down to an energy around $E_h=E_p-n\hbar\omega$ $(0<E_h<\hbar\omega)$ in a cascade of n jumps. Further relaxation is due to interaction with acoustic phonons, and tends to leave the electrons in a roughly thermal distribution at the bottom of the conduction band. If recombination and capture are sufficiently slow compared to this "acoustic" energy relaxation, the electrons "forget" E_h, and normal photoconductivity prevails. But if electron capture or recombination is not slow compared to acoustic energy relaxation, photoconducting electrons will bear a trace of the energy E_h at which they left the original slowing-down cascade. Due to an appreciable energy dependence of the mobility or the capture probability or due to the momentum-loss mechanism,[18] photoconductivity may then oscillate with energy. In our case, variation of the capture cross section accounts for the observations (see Sec. V).

A noticeable feature of oscillating photoconductivity in the cases we have observed is the strong dependence on temperature. At temperatures greater than about 40 K there seems to be no oscillation. The limit is not well defined and seems to vary with Te concentration. Oscillations appear and are accentuated as the temperature is lowered. This enables us to isolate the oscillatory structure from other less-temperature-dependent effects merely by subtracting spectra taken at slightly different temperatures.

III. FANO RESONANCES IN NEUTRAL CENTERS

The spectra used to investigate neutral centers were from absorption, photoconductivity, and Fourier photoadmittance (FPAS). The centers investigated were S^0, Se^0, Te^0, S_2^0, and Se_2^0.

Figure 1 shows excitation spectra of S^0, Se^0, and Te^0. Both bound excited states and Fano resonances are visible. A, B, and C mark Fano resonances associated with the $1s(T_2)$ state and the phonons f LA (S_1), f TO (S_1), and g TO (Δ_2'), respectively. See also Fig. 2(d). The A resonances are discernible in Fig. 1, but are very weak—which is in accordance with the discussion of the f LA phonon in Sec. II A—and this phonon will not be treated further. In Fig. 6 similar spectra are given for S_2^0 and Se_2^0. Due to the lower symmetry (D_{3d}), direct optical transitions to the $1s(T_2)$ state are replaced by transitions to two states $[1s(E^-)$ and $1s(A_1^-)]$, and so are its Fano replicas.

Figure 7 compares three types of spectra for Te^0 in the continuum region and it will be seen that the general resonance structure is similar in the three cases. There is also grosser structure, e.g., a depression of the photoconductivity curve around 255 meV, to which we will return later in connection with oscillating photoconductivity. The well-defined resonance at $\simeq$219 meV is a suitable starting point for analysis, since it exemplifies several of the points made in Sec. II.

The resonance is markedly asymmetric. The shapes in absorption and photoconductivity are different (note that the absorption spectrum in Fig. 7 is magnified relative to the photoconductivity spectrum for purposes of comparison), and the minimum of the photoconductivity reso-

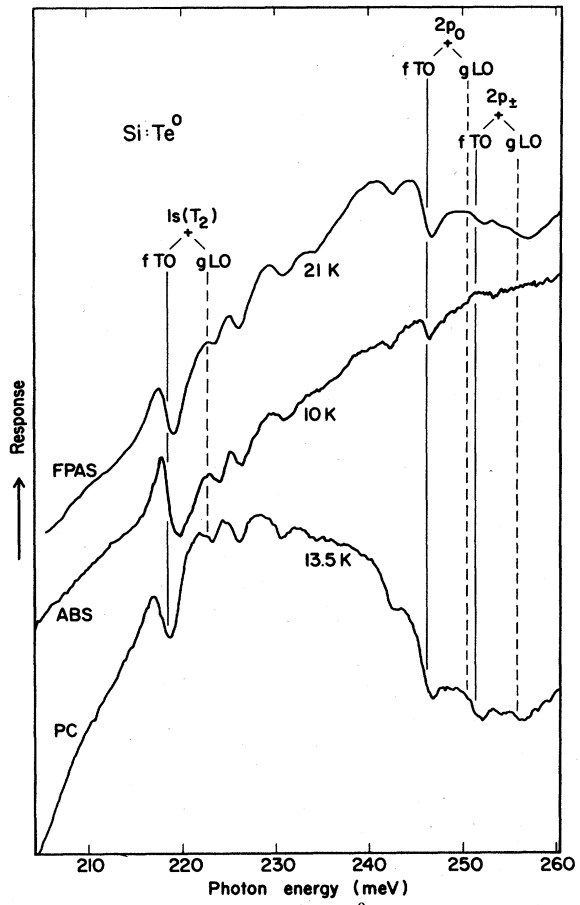

FIG. 7. Continuum spectra for Te^0: FPAS, absorption, and photoconductivity. Spectra have been shifted vertically to avoid confusion.

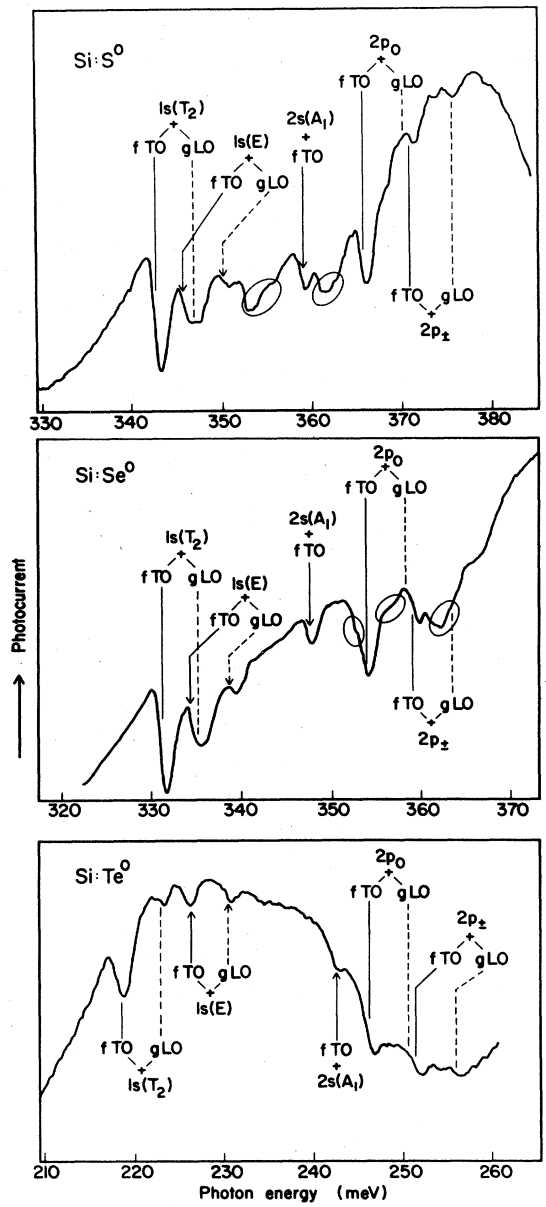

FIG. 8. Photoconductivity continua for S^0, Se^0, and Te^0. The positions of the solid and dashed lines without arrows are obtained by adding the respective phonon energies to the energies of lines below the ionization limit. Arrows indicate resonances associated with bound states not observed in the line spectra. Encircled structures are due to a surface effect.

nance seems to be almost 1 meV lower than that of the absorption resonance. The difference in shape and the shift are in accordance with what was discussed in Sec. II B.

The minimum in the photoconductivity spectrum (always the preferred spectrum for quantitative work) is at 218.9 meV, which is so close to 218.8 meV, the sum of the energies of the $1s(T_2)$ line at 159.7 meV and the f TO phonon (59.1 meV), that there can be no doubt about the assignments. The position of the companion resonance $[1s(T_2)+g$ LO] is also marked in Fig. 7. It corresponds to a resonance roughly one-quarter as strong as the f TO resonance (cf. discussion in Sec. II A).

The intervals between resonances are often not large compared to resonance widths, and this tends to obscure individual shapes—see, e.g., Fig. 9. If observed widths were directly associated with the strength of the continuum-bound interaction (in our case the electron-phonon coupling, $V_{e\text{-ph}}$) as they are in atomic spectra, we might expect considerable interference between adjacent resonances. But since—as we suggest—the widths of observed resonances are mainly due to the phonon bandwidth, it appears justified to regard adjacent resonances as independent of each other. We have seen no shifts of resonance minima such as could arise from interference between resonances.

Figure 8(c) shows photoconductivity spectra for Te^0. Lines marking $(2p_0+f$ TO), $(2p_0+g$ LO), $(2p_\pm+f$ TO), and $(2p_\pm+g$ LO) correspond to specific resonances—the second and third being superposed. Minor structure nearby is perhaps due to $(2s+f$ TO). There remain resonances at 226, 230, and 242 meV—approximate energies being used here merely for identification. The first two are interpreted as a f TO, g LO pair corresponding to an electronic state with a binding energy of 31.6 meV. This energy has been obtained by the method outlined in Sec.

TABLE I. Binding energies of low-lying D^0 and D_2^0 states in chalcogen-doped silicon. Data for Te_2^0 are taken from P. Wagner *et al.* (Ref. 19), results for $1s(E^+)$ and $2s(A_1^{(+)})$ were obtained in the present work, and all other data are from Ref. 1.

	S^0	Se^0	Te^0	S_2^0	Se_2^0	Te_2^0
$1s(A_1^{(+)})$	318.3	306.6	198.8	187.6	206.4	158.2
(A_1^-)				26.5	25.7	25.8
$1s(T_2)$	34.6	34.4	39.1			
(E^-)				31.3	31.3	33.1
$1s(E^{(+)})$	31.6	31.2	31.6	34.4	33.2	
$2s(A_1^{(+)})$	18.4	18.0	15.2	15.3	15.9	

II B, using the two $1s(T_2)$ resonances as reference. The 242-meV resonance has its companion superposed on $(2p_0+f$ TO), and corresponds to an electron state with binding energy 15.2 meV. Neither of these primary states is observed in the line spectra, and they have been assigned $1s(E)$ and $2s(A_1)$, respectively—both of them forbidden in direct optical transitions.

Figure 8 also shows spectra for S^0 and Se^0. Analogous pairs of resonances occur in all three spectra, although overlapping with other resonances and with the structure marked by rings in the figures complicating the S^0 and Se^0 spectra to some extent. The structure marked by rings is common to most of our silicon photoconductors, and is attributed to a surface effect. Derived binding energies for $1s(E)$ and $2s(A_1)$ are given in Table I.

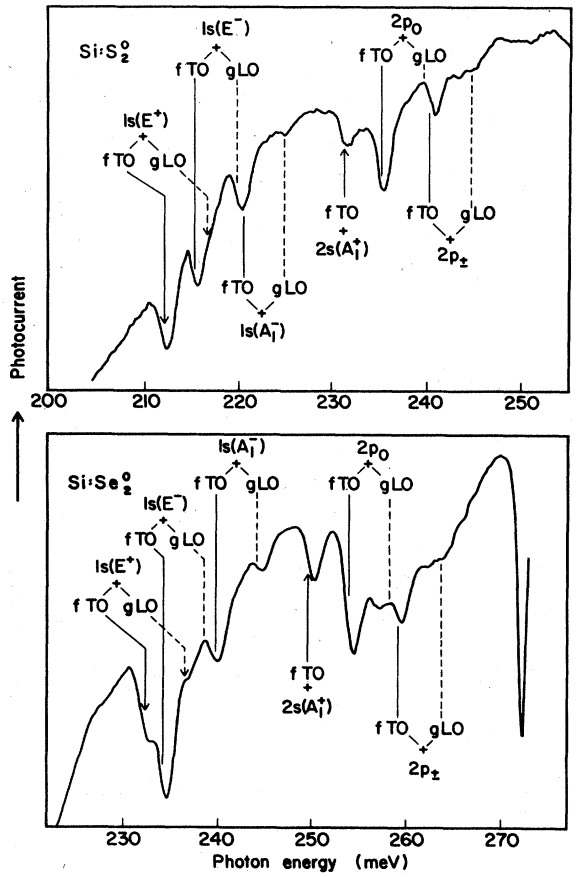

FIG. 9. Photoconductivity continua for S_2^0, Se_2^0. The positions of the solid and dashed lines without arrows are obtained by adding the respective phonon energies to the energies of lines below the ionization limit. Arrows indicate resonances associated with bound states not observed in the line spectra. The dip at 272 meV is due to absorption by the $1s(T_2)$ level of Se^0.

Figure 9 shows photoconductivity spectra for S_2^0 and Se_2^0. Instead of the $1s(T_2)$ resonances of tetrahedral symmetry, we here have resonance pairs for the $1s(E^-)$ and $1s(A_1^-)$ levels of D_{3d} symmetry. They are relatively weaker (compare the multiplicity factors of Sec. II A) and overlap in both cases, but the assignments are clear. The estimate of Sec. II B, that $1s(E^-)$ resonances should be about twice as strong as those associated with $1s(A_1^-)$, and that the f TO resonance should be roughly 4 times as strong as the g LO resonance of the same pair, is in fair agreement with the observed spectra. As before, resonances corresponding to $1s(E^+)$ and $2s(A_1^+)$ can be assigned unambiguously, and binding energies can be derived for these states which are not seen directly in line spectra.

Results are summarized in Table I together with results from spectra below the ionization limit.[1,19] The errors of the binding energies based on Fano resonances are estimated to be ± 0.1 meV for $1s(E)$ in Te^0 and ± 0.4 meV for the other states. Some of the values given here differ from those of Ref. 7 because measurements and evaluation procedures have been improved.

IV. FANO RESONANCES IN Te^0 and Te^+

Figure 10 is an absorption spectrum of Te-doped silicon. The sample was counterdoped with boron to set the Fermi level between the ground levels of Te^0 and Te^+, and spectra of both centers occur in the figure. The sample was epitaxially grown[20] and not of high quality, so that even the $2p_\pm$ level of Te^0 is barely discernible. Note that the spin-valley split $1s(T_2)$ states[21] of Te^+ fall among the Fano resonances of Te^0.

Figure 10 illustrates the comment made in Sec. II B about the negligibility of phonon replicas of bound electronic states. Phonon replicas of the strong $1s(T_2)$ lines in Te^+ would occur in an empty part of the spectrum far below the continuum boundary, and should therefore be detectable even if very weak. Nothing can be seen in Fig. 10. The same applies to the phonon replicas of $1s(T_2)$ in S^+ and Se^+ spectra, and to the phonon replicas of $1s(E^-)$ and $1s(A_1^-)$ in S_2^+ and Se_2^+ spectra—which are not reproduced here.

The first bound state of Te^+ with an identifiable Fano resonance is $2p_0$, and the relevant parts of absorption and

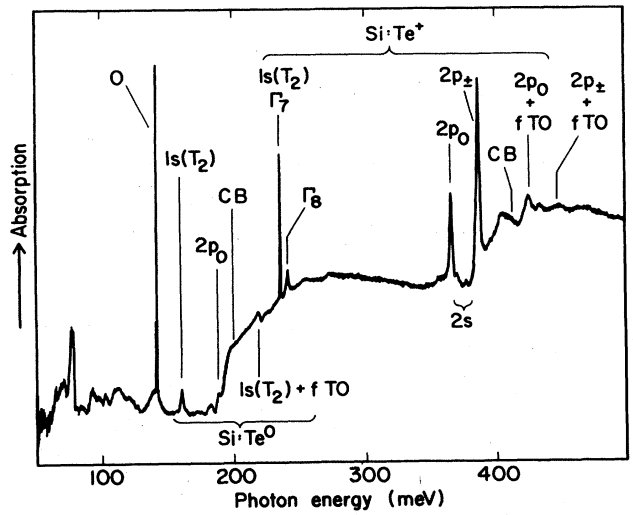

FIG. 10. Absorption spectrum of tellurium-doped silicon showing line spectra of Te^0 and Te^+. Note that the $1s(T_2)$ levels of Te^+ occur among the Fano resonances of Te^0. The resolution is 0.12 meV and the temperature 10 K.

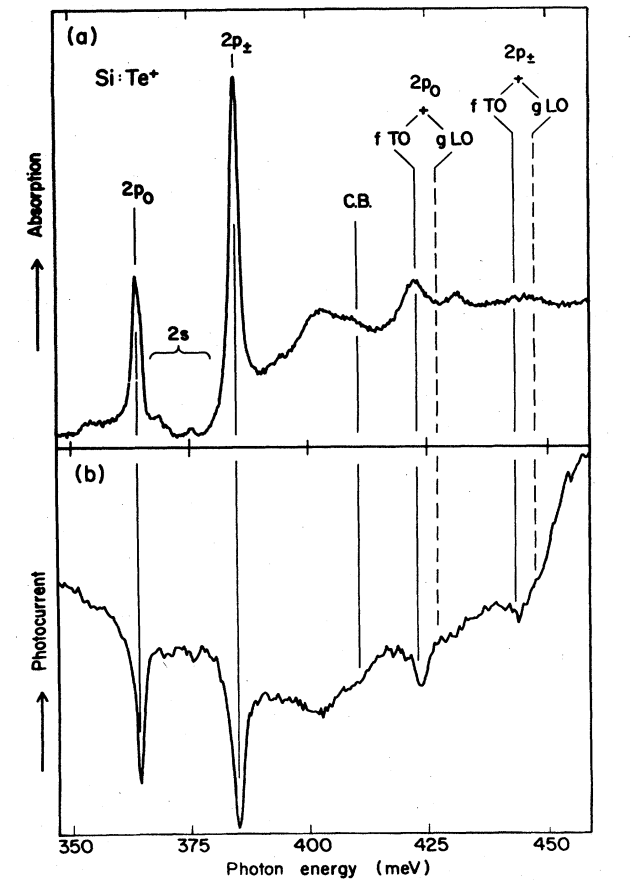

FIG. 11. (a) Magnified part of Fig. 10. The excited states above $2p_\pm$ are smeared out owing to the poor quality of the sample. The positions of expected Fano resonances are marked with solid (f TO) and dashed (g LO) lines. (b) Photoconductivity spectrum of Te^+ covering the same energy range as in (a). The excited levels of Te^+ show up as dips in the continuum of Te^0.

photoconductivity spectra are shown in Fig. 11. The Te^0 continuum is a strong background to the Te^+ spectrum here. Absorption of photons by excitation of bound states in Te^+ results in dips in the Te^0 continuum—an effect which was pointed out in Ref. 1. The shape of resonances above the ionization limit is probably also affected. The $2p_\pm$ resonance is weaker than the $2p_0$ resonance, but it is clearly visible in the photoconductivity spectrum.

V. OSCILLATING PHOTOCONDUCTIVITY AND FPAS SIGNAL

Figure 12(a) shows an absorption spectrum for Te^0, with only minor structure in the continuum part due to Fano resonances described in Sec. III, and a small Te^+ $2p_\pm$ peak at 385 meV. The corresponding photoconductivity spectra in Fig. 12(b) contain major coarse structure in the continuum. Most of the structure increases in amplitude as the temperature is lowered, and is referred to as oscillating photoconductivity. Features such as the dip at 280 meV, the triple dip around 360 meV, and the ascending edge at about 450 meV persist almost unchanged at higher temperature, however. The last two of these features are common to many of our silicon photoconductors, and at least the triple dip around 360 meV seems to be a surface effect—cf. the rings in Fig. 8. The dip at about 280 meV becomes double at the lowest temperature, and the two components coincide in energy with $[1s(T_2)+f\ \text{TO}+f\ \text{TO}]$ and $[1s(T_2)+f\ \text{TO}+g\ \text{LO}]$: this suggests a two-phonon Fano resonance, though such an interpretation is difficult to reconcile with the relatively large strength of this structure and with the absence of two-phonon Fano resonances both in other Te^0 spectra and in spectra for sulfur and selenium centers. However, the concentration of Te was high in these samples, about $10^{17}\ \text{cm}^{-3}$.

The temperature-dependent structure can be separated by a subtraction of spectra, as mentioned in Sec. II C, and the result is shown in Fig. 13. The oscillation has a minimum close to the ionization limit, and a period of 60 ± 1 meV. It decreases in amplitude as the energy increases. The irregularity at 281 meV corresponds to the feature mentioned in the preceding paragraph.

If we attempt to identify the phonons involved in the oscillation of photoconductivity here, we might begin with the same f TO phonons (mean energy 59.1 meV) that were most important in Fano resonances, and find quite good agreement with the observed period. However, the selection rules that led to the f TO and g LO phonons in Sec. II A are here greatly relaxed, because the conducting states between which intervalley transitions occur are up to 300 meV above the band minima and therefore quite widely spread out in $\mathbf{k}$ space. The distribution of the intervalley transition vectors peaks around the f value, but extends up to about half a reciprocal-lattice unit from this mean value. It turns out, though, that the resulting lack of definition of the phonon wave vector does not lead to a particularly large uncertainty in the phonon energy. This may be seen by referring to the phonon frequency distribution of Ref. 14 (which is actually for germanium, but silicon is closely similar): The width of the strong peak due to optical phonons in silicon is about 4 meV, and its

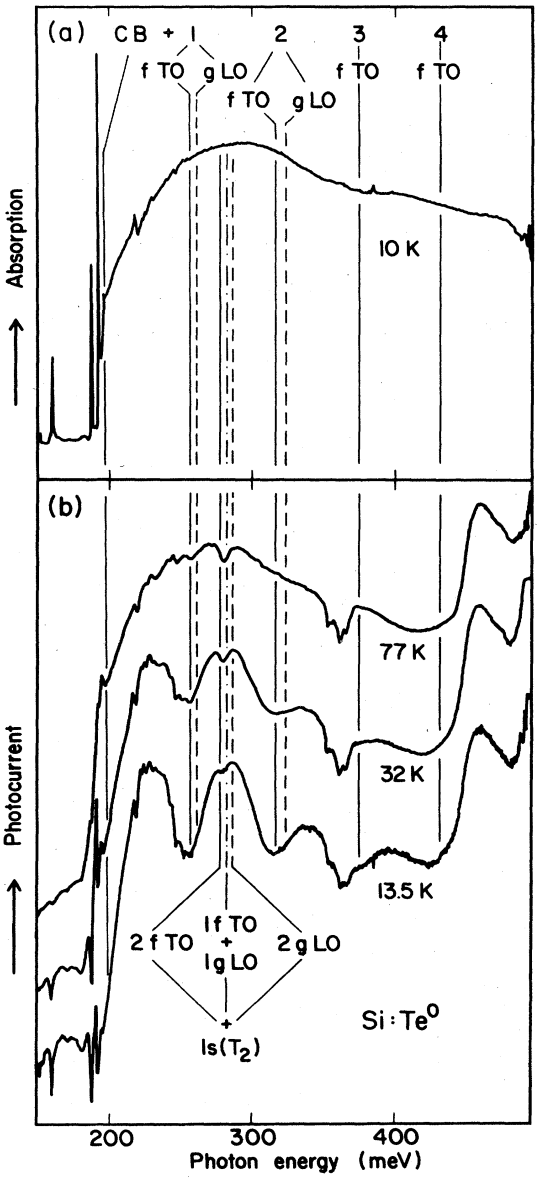

FIG. 12. (a) Absorption and (b) photoconductivity spectra of Te^0 showing how the photocurrent at the lowest temperatures oscillates with a period corresponding to the f TO phonon. The solid line labeled CB marks the ionization limit. The other solid and dashed lines mark energies corresponding to one, two, etc. f TO and g LO phonons above the ionization limit. Lines from below the lowest curve mark a possible assignment of the structure concerned—see text. The resolution is 0.25 meV.

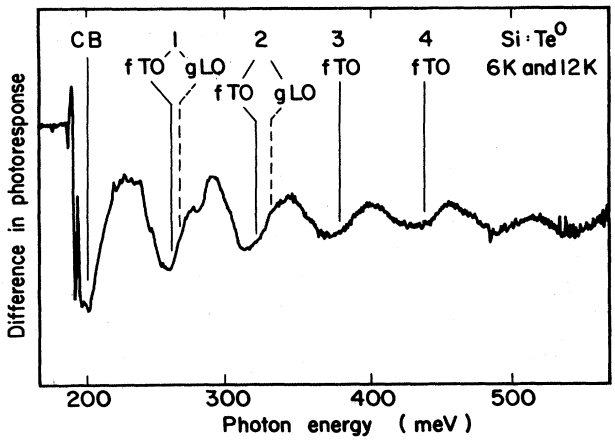

FIG. 13. Oscillating photoconductivity due to Te^0 in silicon. The spectrum was obtained by subtracting the result for 12 K (multiplied by a scaling factor 0.93) from the result at 6 K to separate the strongly temperature-dependent oscillation of photoconductivity from other effects.

mean energy is 60 meV.

As regards the energy-dependent factor in the region of "acoustic" energy degradation within 60 meV of the band minima, this must be such that electrons of energy close to the minimum contribute least to photoconductivity, and such that the effect is accentuated as the temperature decreases. This suggests that the appropriate factor here (see Sec. II C) is the capture of low-energy electrons by impurity centers at low temperatures. It is known that such capture increases very strongly as the temperature decreases, and this has been explained by capture to high excited states of impurity centers, which is not balanced by thermal reemission.[22,23] This means that at low temperatures photoexcited electrons that emerge from the initial "optical" cascade at low energy may be rapidly removed from current transport, while those that must undergo acoustic energy degradation to reach low energy make a large contribution to the photocurrent. At higher temperature, capture becomes slower and oscillations in photoconductivity disappear.

An estimate of timescales involved supports this interpretation of oscillating photoconductivity for Te^0 in silicon. The electron capture cross section of Te^0 was too large to be measured,[24] but its temperature dependence is probably similar to those of S^0 and Se^0. Extrapolating values for S^0 to lower temperature, we find an increase of about 350 times from 77 to 13.5 K. At 13.5 K the capture cross section of S^0 should be of the order of 10^{-12} cm^2. With a concentration of nearly 10^{17} cm^{-3} and an average thermal velocity of 10^6 $cm\,s^{-1}$, this corresponds to a lifetime of thermalized electrons with respect to capture of 10^{-11} s. The figure would of course be lower for Te^0, with its larger cross section, and evidently not long compared to the thermalization time. The increase of 350 times in the capture lifetime when the temperature is raised to 77 K, together with a decrease in the thermalization time, seems to account adequately for the disappearance of the oscillating photoconductivity long before the higher temperature is reached.

It will be seen that the minima of the oscillations are slightly shifted to the left of the lines marking CB, [CB + 1×(f TO)], and so on. The energy at which the photocurrent at 6 K first falls sharply below the photocurrent at 12 K is also a few meV below the ionization limit. This indicates that impurity states a few kT below the ionization limit are from the present point of view indistinguishable from ionized states. This is in accordance

with the high probability of "hopping" between impurities for these extensive states at the relatively high tellurium concentration concerned here, and the high probability of thermal excitation to the conduction band.

Figure 14 shows FPAS (Ref. 8) spectra for a Schottky diode at different temperatures, the center concerned again being Te^0. Oscillatory behavior at the lowest temperature is very evident. Whereas homogeneously doped samples of millimeter thickness were used for the results of Figs. 12 and 13, the diffusion depth of tellurium in Schottky diodes used for FPAS measurements was only a few micrometers, with a concentration of tellurium atoms at the surface of a few times 10^{16} cm^{-3}. The active FPAS region moves farther into the crystal as the temperature decreases, which explains why the surface effect around 360 meV disappears at 18.5 K. A difference relative to the photoconductor is that the first minimum is now above the ionization limit. The reason for this difference is not understood, but it is obvious that the FPAS situation is more complicated and no doubt affected by the large electric field in the active region of the diode.

VI. SUMMARY

Resonance structure in the continuum part of photoexcitation spectra of chalcogen donors in silicon are presented and interpreted in terms of the electron-phonon interaction coupling the electronic continuum states to bound states of the donor. These resonances are attributed to interference effects in the initial excitation process and are thus not related to the subsequent carrier transport. The resonance structure enables us to determine binding energies of excited states that are not accessible from the ground state in optical absorption. Our theoretical model suggests that absorption and photoconductivity spectra differ since two interacting continua—the electronic conduction band and the band of phonons with a bound electron in an excited state—are both possible final-state channels of the excitation. Furthermore, the width of the resonance structure appears to be essentially determined by the width of the narrow band of resonant phonons while the effect of the electron-phonon interaction is weak. This is consistent with the fact that nonresonant phonon replicas have not been observed for chalcogen centers.

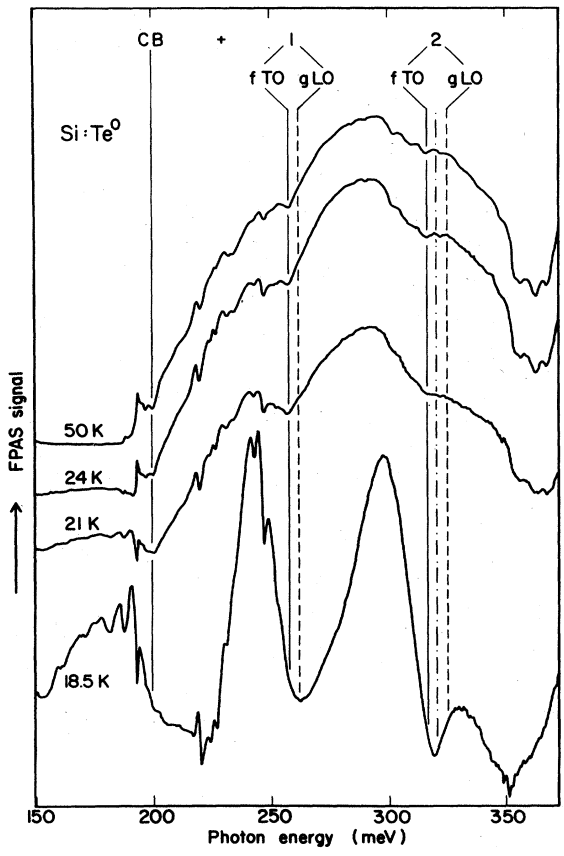

FIG. 14. FPAS—spectra of Te^0 showing oscillatory behavior at low temperatures. CB marks the ionization limit and the other solid and dashed lines the addition of one or more phonon energies. The resolution is 0.5 meV.

ACKNOWLEDGMENTS

The authors gratefully acknowledge valuable discussions with C. O. Almbladh, L. Hedin, and J. C. Inkson. C. Holm is gratefully acknowledged for supplying Te-doped samples and P. Wagner for providing results prior to their publication.

APPENDIX A: PHONON ENERGIES IN SILICON

Phonon energies in silicon have been determined using inelastic neutron scattering by Dolling[25] and by Nilsson and Nelin.[26] For the optical phonons which are of particular interest here, the errors in the former case were estimated to be about 2.5%, while for the few data of the latter case they are given as 0.3%. The data for acoustic branches of the phonon dispersion relations from both sources are much more complete and accurate. The errors of the early work on optical phonons[25] can be reduced considerably by adjusting phonon dispersion curves of a given general shape to provide a best fit to the complete data, aided by the few more accurate data which are available (from Ref. 26, and for zero wave vector from the Raman measurements of Hart *et al.*[27]). Asche and Sarbei[12] have employed such a procedure, using families of theoretical curves for interpolation, but with a less strict selection of data than here. We have carried out an interpolation with the aid of accurately known dispersion relations for optical phonons in germanium[14] which have been shown to be in almost constant ratio to those of silicon.[26] The optical phonon energies of Dolling were increased by 0.6% to give an approximate conversion from 300 to 80 K (this difference being taken from Ref. 26). The result of the interpolation is shown in Fig. 15, where the f and g wave vectors (see Sec. II A) are indicated. The energies of the important f and g phonons have thus been determined as follows: f TO(S_1), 59.1±0.2 meV; f LA(S_1), 48.1±0.2 meV; and g LO(Δ_2'), 63.9±0.2 meV. These values differ somewhat from those of Asche and Sarbei[12] and those of Portal *et al.*[28] (which were used in Ref. 7). The value for the important f TO phonon agrees

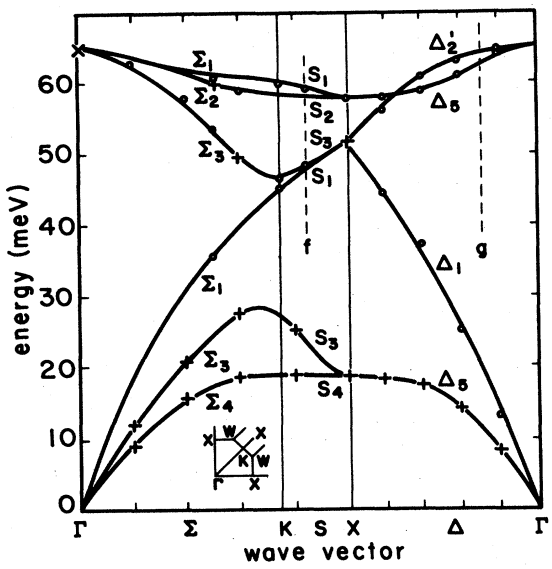

FIG. 15. Dispersion curves for phonons in silicon, derived as explained in the text. Results of Dolling (Ref. 25) are denoted by ●, of Nilsson and Nelin (Ref. 26) by +, and of Hart *et al.* (Ref. 27) by ×.

with the value given by the measurements of Butler *et al.*[9] on the anomalous broadening of a Si:Bi line (cf. Sec. II A). The value for the f LA phonon is in agreement with our own[1] observations on the anomalously broad $2p_0$ levels of S_2^+ and Se_2^+, and in fact indicates why the broadening is greater in S_2^+, since that case is closer to resonance with a phonon of the energy quoted here.

APPENDIX B: ABSORPTION AND PHOTOCONDUCTIVITY SPECTRUM

Here we will only give a rather brief outline of the evaluation of the absorption and photoconductivity spectra. For further details we refer the reader to Ref. 16. With the zero of energy taken at the donor ground-state energy E_i, Eq. (1) may be rewritten as

$$I_a(\omega)=-2\,\mathrm{Im}\left\langle i\left|T\frac{1}{\omega-H+i\eta}T\right|i\right\rangle . \tag{B1}$$

T is the optical dipole transition operator and H the full Hamiltonian, that includes both U and $V_{e\text{-ph}}$, $H=H_0+V_{e\text{-ph}}+U$. Inserting a complete set of states

$$\left\{|\phi_0\rangle\langle\phi_0|+\int d\epsilon\,|\phi_\epsilon\rangle\langle\phi_\epsilon|\right\}$$

to the left and right of the Green's function $G^+(\omega)=(\omega-H+i\eta)^{-1}$ in Eq. (B1), we need to evaluate the matrix elements of G^+. Introducing $G_0^+=(\omega-H_0+i\eta)^{-1}$, we may expand G^+ as

$$G^+=G_0^+ +G_0^+VG_0^+ +G_0^+VG_0^+VG_0^+ +\cdots ,$$

where $V=V_{e\text{-ph}}+U$. We have

$$\begin{aligned}G_0^+VG_0^+V\,|\phi_0\rangle&=G_0^+(UG_0^+U+V_{e\text{-ph}}G_0^+V_{e\text{-ph}})\,|\phi_0\rangle\\&=\frac{1}{\omega-\epsilon_0+i\eta}\left[\int d\epsilon\frac{|U(\epsilon)|^2}{\omega-\epsilon+i\eta}+\int d\epsilon\frac{|V_{e\text{-ph}}(\epsilon)|^2}{\omega-\epsilon+i\eta}\right]|\phi_0\rangle\\&=\frac{1}{\omega-\epsilon_0+i\eta}\Sigma(\omega)\,|\phi_0\rangle .\end{aligned}$$

Here, $V_{e\text{-ph}}(\epsilon)=\langle\phi_0|\,V_{e\text{-ph}}\,|\phi_\epsilon\rangle$, $U(\epsilon)=\langle\phi_0|\,U\,|\phi_\epsilon\rangle$, and we have introduced the self-energy $\Sigma(\omega)$. $(G_0^+V)^2$ thus acts as a scalar on $|\phi_0\rangle$ and we may sum the series

$$\begin{aligned}&[1+(G_0^+V)^2+(G_0^+V)^4+\cdots]\,|\phi_0\rangle\\&\qquad=\frac{\omega-\epsilon_0}{\omega-\epsilon_0-\Sigma(\omega)}\,|\phi_0\rangle ,\end{aligned}$$

and find

$$\langle\phi_0|\,G^+\,|\phi_0\rangle=\frac{1}{\omega-\epsilon_0-\Sigma(\omega)} . \tag{B2}$$

Similarly we have

$$\begin{aligned}\langle\phi_0|\,G^+\,|\phi_\epsilon\rangle&=\langle\phi_0|\,(G_0^+ +G_0^+VG_0^+VG_0^+ +\cdots)VG_0^+\,|\phi_\epsilon\rangle\\&=\langle\phi_0|\,(1+G_0^+VG_0^+V+\cdots)G_0^+\,|\phi_0\rangle\frac{V_{e\text{-ph}}(\epsilon)}{\omega-\epsilon+i\eta}\\&=\frac{1}{\omega-\epsilon_0-\Sigma(\omega)}\frac{V_{e\text{-ph}}(\epsilon)}{\omega-\epsilon+i\eta} ,\end{aligned} \tag{B3}$$

$$\langle\phi_\epsilon|\,G^+\,|\phi_0\rangle=\frac{1}{\omega-\epsilon_0-\Sigma(\omega)}\frac{V_{e\text{-ph}}^*(\epsilon)}{\omega-\epsilon+i\eta} , \tag{B4}$$

and

$$\langle \phi_\epsilon | G^+ | \phi'_\epsilon \rangle = \frac{V^*_{e\text{-ph}}(\epsilon)}{\omega-\epsilon+i\eta} \frac{1}{\omega-\epsilon_0-\Sigma(\omega)} \frac{V_{e\text{-ph}}(\epsilon')}{\omega-\epsilon'+i\eta} . \tag{B5}$$

Writing $\Sigma(\omega)=\Delta(\omega)-i\Gamma(\omega)$, where

$$\Delta(\omega)=\mathrm{P}\int d\epsilon \frac{|V_{e\text{-ph}}(\epsilon)|^2+|U(\epsilon)|^2}{\omega-\epsilon}$$

and (B6)

$$\Gamma(\omega)=\pi|V_{e\text{-ph}}(\omega)|^2+\pi|U(\omega)|^2 = \Gamma_1(\omega)+\Gamma_2(\omega)$$

(P denotes the principle part) and introducing

$$T'_0=T_0+\mathrm{P}\int d\epsilon \frac{T_\epsilon V^*_{e\text{-ph}}(\epsilon)}{\omega-\epsilon} , \tag{B7}$$

$E=\omega-\epsilon_0-\Delta$, and the Fano parameter q by

$$q=\frac{1}{\pi}\frac{T'_0}{V^*_{e\text{-ph}}(\epsilon)T_\epsilon} , \tag{B8}$$

we obtain Eq. (4) after some lengthy but straightforward manipulations.

For the T^+ operator in Eq. (3) for the photoconductivity spectrum,

$$I_{\mathrm{pc}}(\omega)=2\pi\int d\epsilon |\langle \phi_\epsilon | T^+ | i \rangle|^2 \delta(E_i+\omega-\epsilon) , \tag{3}$$

we have

$$T^+=V+VG^+V , \tag{B9}$$

where V contains $V_{e\text{-ph}}$ and U, and also the interaction with the radiation field. To lowest order in the radiative interaction T, the scattering amplitude becomes

$$\tau_{\epsilon i}=\langle \phi_\epsilon | (1+VG^+)T | i \rangle \tag{B10}$$

which, after again inserting a complete set of states, may be evaluated along the same lines as in the case of absorption.

*Present address: ASEA Research and Innovation, Optical Sensors, S-721 83 Västerås, Sweden.

[1]E. Janzén, R. Stedman, G. Grossmann, and H. G. Grimmeiss, Phys. Rev. B **29**, 1907 (1984).
[2]U. Fano, Phys. Rev. **124**, 1866 (1961).
[3]A. Onton, Phys. Rev. Lett. **22**, 288 (1969).
[4]G. D. Watkins and W. B. Fowler, Phys. Rev. B **16**, 4524 (1977).
[5]R. Baron, M. H. Young, and T. C. McGill, Solid State Commun. **47**, 167 (1983).
[6]R. G. Humphreys, P. Migliorato, and G. Fortunato, Solid State Commun. **40**, 819 (1981).
[7]E. Janzén, R. Stedman, and H. G. Grimmeiss, in *Proceedings of the 16th International Conference on the Physics of Semiconductors, Montpellier, 1982,* edited by M. Averous (North-Holland, Amsterdam, 1983), p. 125.
[8]E. Janzén, K. Larsson, R. Stedman, and H. G. Grimmeiss, J. Appl. Phys. **53**, 7520 (1982).
[9]N. R. Butler, P. Fisher, and A. K. Ramdas, Phys. Rev. B **12**, 3200 (1975).
[10]H. W. Streitwolf, Phys. Status Solidi **37**, K47 (1970).
[11]M. Lax and J. L. Birman, Phys. Status Solidi **49**, K153 (1972).
[12]M. Asche and O. G. Sarbei, Phys. Status Solidi B **103**, 11 (1981).
[13]W. Harrison, Phys. Rev. **104**, 1281 (1956).
[14]G. Nelin and G. Nilsson, Phys. Rev. B **5**, 3151 (1972).
[15]A. P. Jauho and P. Minnhagen, J. Phys. C **17**, 4369 (1984).
[16]C. O. Almbladh and L. Hedin, in *Handbook of Synchrotron Radiation,* edited by E. E. Koch (North-Holland, Amsterdam, 1983), Vol. 1.
[17]Y-C. Chang and T. C. McGill, Solid State Commun. **47**, 171 (1983).
[18]Y. Marfaing, *Handbook of Semiconductors* (North-Holland 1980), Vol. 2, p. 417.
[19]P. Wagner, C. Holm, E. Sirtl, R. Oeder, and W. Zulehner, *Advances in Solid State Physics XXIV,* edited by P. Grosse (Vieweg, Braunschweig, 1984), p. 191.
[20]Some of the tellurium samples were fabricated by C. Holm.
[21]H. G. Grimmeiss, E. Janzén, and K. Larsson, Phys. Rev. B **25**, 2627 (1982).
[22]M. Lax, Phys. Rev. **119**, 1502 (1960).
[23]V. N. Abakumov, V. I. Perel, and I. N. Yassievich, Fiz. Tekh. Poluprovodn. **12**, 3 (1978) [Sov. Phys.—Semicond. **12**, 1 (1978)].
[24]H. G. Grimmeiss, E. Janzén, H. Ennen, O. Schirmer, J. Schneider, R. Wörner, C. Holm, E. Sirtl, and P. Wagner, Phys. Rev. B **24**, 4571 (1981).
[25]G. Dolling, in *Inelastic Scattering of Neutrons in Solids and Liquids* (IAEA, Vienna, 1963) Vol. II, p. 37.
p. 37.
[26]G. Nilsson and G. Nelin, Phys. Rev. B **6**, 3777 (1970).
[27]T. R. Hart, R. L. Aggarwal, and B. Lax, Phys. Rev. B **1**, 638 (1970).
[28]J. C. Portal, P. Perrier, C. Houlbert, S. Askenazy, R. I. Nicholas, and R. A. Stradling, J. Phys. C **12**, 5121 (1979).